Materiales de Construcción 75 (359)
July-September 2025, e386
ISSN-L: 0465-2746
https://doi.org/10.3989/mc.2025.389424

Electrical resistivity tomography for moisture dynamics analysis in historic adobe structures: practical case of Casa Terán, Aguascalientes, México

R. Padilla-Ceniceros[a,d] ✉, J. Pacheco-Martínez[a], W. H. Herrera León[b], M. Hernández-Marín[a], R. A. López-Doncel[c], J. G. Villanueva Clavel[a], H. Luna-Villavicencio[d]

a. Departamento de Ingeniería Civil, Centro de Ciencias del Diseño y de la Construcción, Universidad Autónoma de Aguascalientes, (Aguascalientes, Mexico)
b. Departamento de Ingeniería, Instituto Tecnológico Nacional de México/Instituto Tecnológico de Tepic, (Nayarit, Mexico)
c. Instituto de Geología, Universidad Autónoma de San Luis Potosí, (San Luis Potosí, Mexico)
d. Facultad de Ingeniería, Universidad Panamericana, (Aguascalientes, México)
✉: raudelpc@gmail.com

Received 11 July 2024
Accepted 26 February 2025
Available on line 11 March 2026

ABSTRACT: This study employs Electrical Resistivity Tomography (ERT) to analyze moisture dynamics in an adobe wall of Casa Terán, a historic building in Aguascalientes, Mexico. By modifying the ERT technique with medical electrostimulators, the study identifies the causes and propagation patterns of moisture based on material properties. Previous interventions are also reviewed to determine the materials used. By integrating geotechnical and geoelectrical data, the study evaluates subsurface saturation levels, moisture propagation zones, and potentially weak areas in the wall. The correlation of ERT derived models with intervention images helps interpret the influence of construction materials on moisture propagation. This research is crucial for conserving historic structures and mitigating moisture-induced damages.

KEY WORDS: ERT; Moisture dynamics; Moisture damage; Rising damp; Casa Terán.

Citation/Citar como: Padilla-Ceniceros R, Pacheco-Martínez J, Herrera León WH, Hernández-Marín M, López-Doncel RA, Villanueva Clavel JG, Luna-Villavicencio H. 2025. Electrical resistivity tomography for moisture dynamics analysis in historic adobe structures: practical case of Casa Terán, Aguascalientes, México. Mater. Construcc. 75(359):e386. https://doi.org/10.3989/mc.2025.389424

RESUMEN: *La tomografía de resistividad eléctrica para el análisis de la dinámica de humedad en estructuras históricas de adobe: caso práctico de Casa Terán, Aguascalientes, México*. Este estudio emplea la Tomografía de Resistividad Eléctrica (ERT) para analizar la dinámica de la humedad en un muro de adobe de la Casa Terán, un edificio histórico en Aguascalientes, México. Al modificar la técnica ERT con electroestimuladores médicos, el estudio identifica las causas y los patrones de propagación de la humedad según las propiedades del material. También se revisan intervenciones previas para determinar los materiales utilizados. Integrando datos geotécnicos y geoeléctricos, el estudio evalúa los niveles de saturación del subsuelo, las zonas de propagación de humedad y las áreas potencialmente débiles en el muro. La correlación de los modelos derivados de ERT con imágenes de intervenciones ayuda a interpretar la influencia de los materiales de construcción en la propagación de la humedad. Esta investigación es crucial para conservar estructuras históricas y mitigar los daños inducidos por la humedad.

PALABRAS CLAVE: ERT; Dinámica de la humedad; Daños por humedad; Humedad ascendente; Casa Terán.

1. INTRODUCTION

1.1. Casa Terán

Casa Terán is a two-level building declared as a national historic monument in 1986, built mostly with adobe walls (1). Since the beginning of its construction in 1775 until 1986, there is no record of important remodeling or restoration work. However, in 1991 restoration works were carried out respecting the original architectural design (1). This intervention consisted of a full rehabilitation work on the floor of both levels, highlighting the restoration of low ceilings, reintegration of mural painting and ceilings, as well as the entire electric and hydraulic installations.

In July 2012 the building was damaged due to an explosion generated by gas concentration, causing the collapse of 30% of the building (2). In consequence, by 2013 a reconstruction work was carried out involving a technique used in archaeology called “Anastylosis”, which consists of repairing the building using its original remains scattered in situ. Furthermore, the application of this technique included a detailed photographic record of the ruined building (Figure 1), in order to identify the types of materials and their characteristics, as well as the construction techniques used in the original construction and the intervention process. Since its first intervention in 1991, moisture problems were reported in several walls of the building.

Figure 1. Images obtained from the interior of the Casa Terán in 1991. Humidity problems are observed in the lower part of the walls, inferior stairs and structural elements. a) Stable area, currently a covered patio with a cinema area. b) Stairs over the corridor on one side of patio 2.

1.2. Moisture problems in historic buildings

Dampness, as in countless historic buildings worldwide, can cause a range of damage from minor to truly destructive. In Casa Terán two main types of dampness have caused significant damage mainly to the walls of the building. Water from the ground on which the building is built travels up the walls through capillary forces causing not only the formation of stains on the walls but also softening of the original material, formation of saltpeter (salt crystallization), discoloration, and even detachment of material. Another important source of dampness comes from the inside of the walls caused by leaks in the already aging and unusable plumbing system that extends throughout the house, causing the same damage as capillary water but at different levels of the walls. A very important factor that favors the distribution of moisture damage is the material with which the house was built, as its walls are made of adobe, a highly porous material, which easily allows moisture to pass through it and which is also very soft and not very compact.

Water is typically the primary challenge for the preservation of architectural heritage (3-5), making it crucial to study moisture in walls for their conservation. Water and moisture in general can gain access to historic buildings through various processes and means of transport such as a) capillarity, b) condensation, c) pipe leaks, d) rain infiltration, and e) flooding (4-8). High levels of moisture may accelerate material degradation when for example temperature is below 0° due to freeze-thaw cycles (9, 10), or in presence of soluble salts (salt crystallization) (11-15), through chemical processes (e.g. dissolution and hydrolisis), biological attacks (e.g. bio-colonisation) (16-18), metal corrosion, and driven rain (19-21).

Moisture is one of the main agents promoting deterioration in buildings, including architectural heritage. Moisture in buildings can occur through any of the following mechanisms: a) capillarity, b) condensation, c) leaks in pipes, d) rain seepage, e) flooding, runoff and accumulation (4, 5, 8). For buildings in the center of the city of Aguascalientes, middle Mexico, the biggest moisture problems are related to rising dampness by capillarity from the subsoil, since according to Gómez Serrano (22) most of the old buildings, built between the 18^{th}-19^{th} centuries were settled on or next to orchards and irrigation ditches, which caused serious deterioration in the buildings and differential settlements. The water sources that have been most frequently identified affecting buildings due to moisture concentration are leaks derived from the deterioration of the hydraulic installations, as well as well as old waterholes that continue having a shallow water table by the prescence of a perched aquifer, according to users of buildings in the downtown area of the city. The damage caused to buildings is especially critical due to the type of materials and construction systems used. For example, Casa Terán has adobe walls without foundations, which exacerbates the problem.

Capillary moisture in adobe walls is a common and complex phenomenon (23, 24). It manifests with visible signs such as discoloration and structural problems, arising from physical, chemical, and biological reactions to moisture exposure (25, 26). Giaccone (27) explains that, at a macroscopic level, walls affected by rising damp can be divided into three distinct sections: (a) a lower section with a high moisture content, (b) an upper section where water does not cause surface pathologies and the moisture content is comparatively low, and (c) an intermediate section where the moisture level varies cyclically according to environmental conditions, bounded by an upper (MaxBIh) and a lower (MinBIh) water mark, as shown in Figures 2a and 2b. That is two borderlines (MinBIh and MaxBIh), within which, the rising front ranges periodically. These Borderlines identify Iso-humidity (BIh) surfaces, so called because each point of masonry belonging to them has the same content of water. Franzoni (19, 26-28) presents a diagram describing the four factors that determine the height of rising damp. Figure 2 combines these ideas to provide a more comprehensive diagram of the capillary phenomenon in masonry walls.

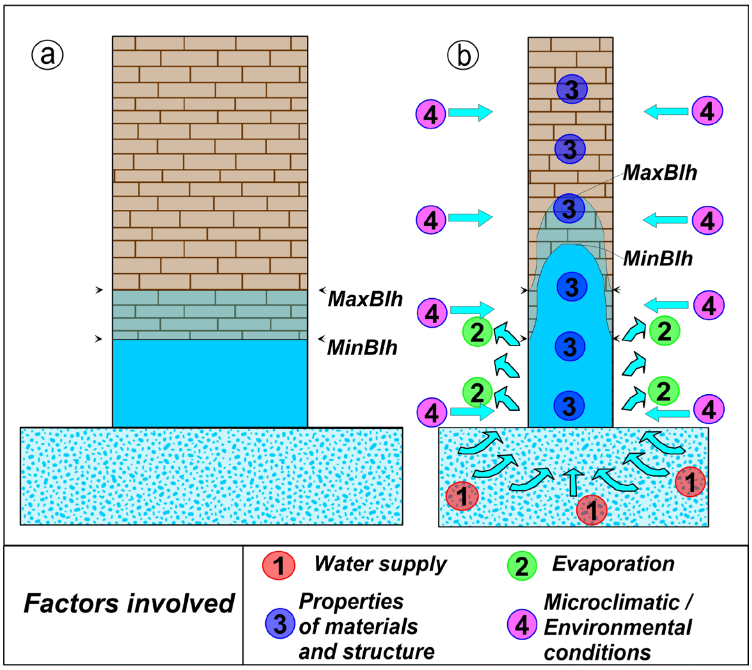

FIGURE 2. Dynamics of capillary water rise in a masonry. a) wall elevation view with identification of lowest (MinBIh) and highest (MaxBIh) water internal marks. b) Section of the wall with the four factors involved with identification of lowest (MinBIh) and highest (MaxBIh) water external marks. Modified from the approaches of Franzoni, Giaconne (19, 26-28).

In the continuous flow from the lower part of the wall to the upper part of the damp front, four main factors are involved: water supply from the ground, evaporation, and the properties of the construction materials (including pore quantity, size, connectivity, and tortuosity, see Figure 2b), and the microclimatic or environmental conditions (19, 26-28). In walls where the flow is abundant, combined with an extremely porous material and fine pores, and the absence of evaporation, rising damp can reach significant heights (26).

The pore size and distribution determine the rise of moisture in walls (19, 26-28). According to Rirsch and Zhang (29), pore size in materials significantly affects the height of the moisture front. In materials with pores of 0.1 mm, the elevation is 0.14 cm, while in those with pores of 0.01 mm, the elevation can reach up to 1.4 m. In the case of brick, the pore size can be as small as 0.001 mm, suggesting that the moisture front could be considerably elevated. It is necessary to analyze the porosity data for adobe.

The aim of this study is to investigate the cause and propagation of humidity in one of the most severely affected walls of the building. Leveraging data gathered during the 2013 intervention, we possess valuable insights into the construction system, materials employed in the studied wall, and the characteristics of the underlying soil. This makes it an exemplary case for comprehending the dynamics of moisture origination and dissemination within such walls, employing non-intrusive methodologies.

Electrical Resistivity Tomography (ERT) is a geophysical technique used to determine the electrical properties of subsoil resulting in an electrical resistivity section. Since soil electrical resistivity depends on a) minerals of solid particles, b) porosity, c) water quantity in the soil pores, and d) type and quantity of dissolved salts in the water that is in the pores, ERT measurements are particularly useful for identifying zones within the subsoil that have higher water content, assuming the other factors remain relatively constant throughout the studied section (30, 31).

The research entails assessing the dynamic moisture behavior through 2D and 3D electrical resistivity models generated via ERT measurements conducted in both the soil and the wall. Additionally, data from the subsoil and the materials and construction techniques employed during the 2013 intervention are integrated. Through the ERT models, regions exhibiting the highest moisture concentrations correlated with areas of lowest resistivity are delineated, alongside identifying the maximum height reached by the moisture front within the wall.

2. MATERIALS AND METHODS

The overall methodology involved describing the Casa Terán building, with a particular focus on the wall where in situ measurements were conducted. A brief explanation of the tests used in soil mechanics was provided, along with a description of the properties of the superficial strata. Additionally, a sequence of electrical tomography measurements was performed and analyzed to determine the origin and dynamics of moisture. Finally, the processing of the ERT data was explained, accompanied by images obtained from the 2013 intervention (see the flowchart in Figure 6).

2.1. Casa Terán

Casa Terán is a construction in the Baroque and Neoclassical style. It consists of tiled floors of fired brick, adobe walls of variable thicknesses, mostly between 0.5 and 0.7 m, wooden and brick beamed ceilings. Initially it contained three patios, a hall, thirteen rooms on the lower level, four on the upper level, a corral, a stable, a haystack and a garage. The wall under study corresponds to the area directly affected by the 2012 explosion, located between the dining room and the coffee shop as shown in Figure 3. The part of the wall studied is 6.07 m long, with a constant height of 5.61 m but a variable thickness, having 0.75 and 0.71 m to the east and west, respectively. As a result of the explosion, the wall partially collapsed, losing around 40% of its original composition (Figure 3a).

Before the explosion, the wall had moisture ascending from the subsoil (a diagonal stain on the wall is indicated in Figure 3a), thus, in the first intervention of 1991, knapen siphons (systems of tubes introduced to the wall at an angle to reduce humidity) were placed in the wall every 0.80 m and at 0.5 above the finished floor level, staggered pattern on both sides. For this intervention, the wall was completed with adobe blocks similar to the original ones, they were bonded with slaked lime mortar and were placed flattened with slaked lime and sand to create compatibility between the materials and to favor the proper transpiration of the wall.

After the 2013 intervention, the wall was composed of the following materials (Figures 3 and 4): 1) adobe blocks of 0.09x0.2x0.4 and 0.09x0.4x0.4 m from the original wall joined with slaked lime mortar and small elongated stones, 2) adobe blocks of 0.09x0.2x0.4 and 0.09x0.4x0.4 m in the reconstructed area of the wall after 2013, joined with slaked lime mortar and small elongated stone, 3) volumes of 0.6x1x0.28 m of fired brick with dimensions of 0.07x0.14x0.28 m joined with cement mortar, used as connection elements between the study wall and the cross wall of axis D (Figure 5a and Figure 4d) from 1.1 m in height and at every 1 m in height (Figure 3b). This practice is common in Central Mexico, as it is believed to ensure a strong connection between the perpendicular walls made of adobe blocks. 4) Fired brick of 0.04x0.13x0.26 m in the lower part of the wall with a tambourine rigging (Shiner course) between 0 to 2 m high as wall consolidation elements (Figures 3c and 4d), 5) prismatic elements of the locally named matacán (fine-grained white sandstone) between 0 and 1 m high as wall consolidation material (broken fired brick bonded with lime mortar). Consolidation elements are materials used to reintegrate a weakened wall due to the loss of material or the occurrence of fractures or cracks.

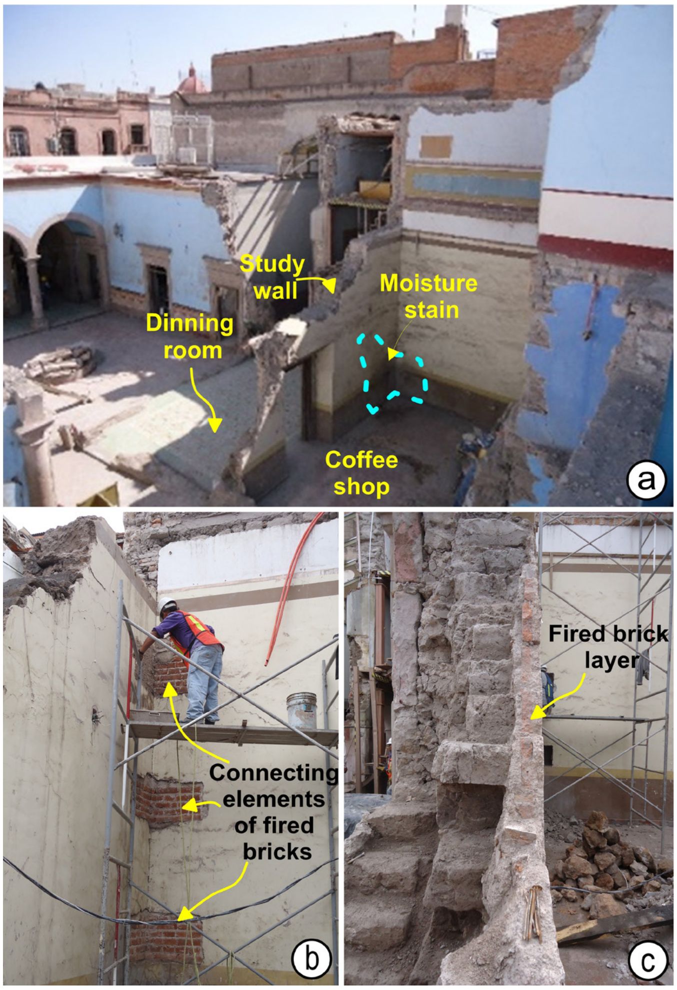

Figure 3. Images after the 2012 explosion. a) View of the first patio, dining room, and coffee shop after debris removal. b) Elaboration of connecting elements of fired bricks between walls. c) Section of the partially collapsed wall (32).

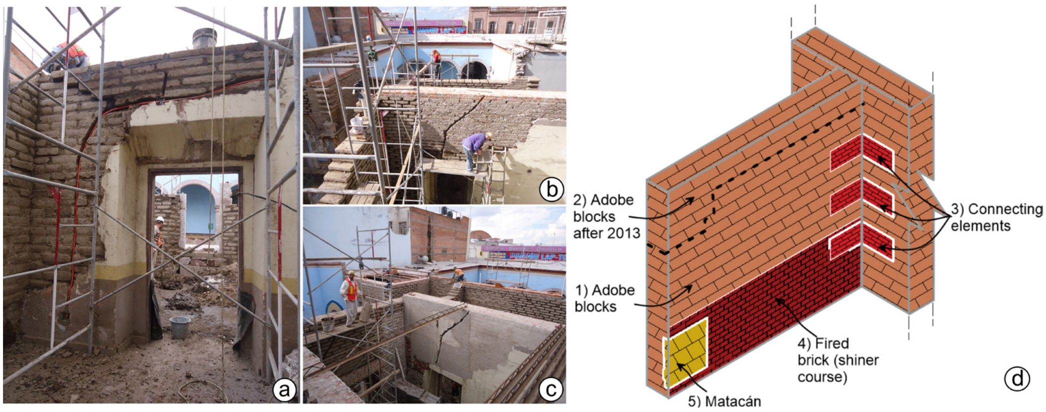

Figure 4. Reconstruction of dividing wall. a) Placement the first rows of adobe over the door. b) Insertion of mortar and small elongated stones joints. c) Reconstructed wall covered with slaked lime mortar (32). d) Drawing showing the different materials that make up the study wall.

2.2. Subsoil geotechnical properties

From three disturbed samples obtained from three boreholes using the open-pit (OP) technique (Figure 5a), the geotechnical properties of the subsoil beneath the Casa Terán structure were determined. In addition, to obtain the resistance parameters, dynamic cone penetration (DCP) tests were conducted.

The methods used to characterize the soil layers are standardized and described in the standards ASTM D4318-17e1, ASTM D6913M-17, ASTM D4959-24, and ASTM D2487-17 (33-36). From the OP, only two layers of soil with variable thicknesses are observed, which are summarized as follows:

Layer 1: This surface layer consists of dark brown soil classified by the Unified Soil Classification System (USCS) as a low compressibility silt (ML) with 4 % gravel, 39 % sand, and 57 % fine. The liquid and plastic limits are 40.1 % and 28.1 %, respectively. The natural water content is 22.8 %, and the bulk density is 14.71 kN/m³. This layer deepens from the surface to 1.1 meters in borehole 1, 2.0 meters in borehole 2 and 2.10 meters in borehole 3.

Layer 2: This layer consists of light brown soil classified by the USCS as clayey sand (SC) with 11 % gravel, 66 % sand, and 23 % fine. The liquid and plastic limits are 38.1 % and 23.5 %, respectively. The natural water content is 11.6 %, and the bulk density is 16.8 kN/m³. This layer´s upper limit is at a depth of 1.1 meters but its lower limit was not reach by the survey.

2.3. ERT measurements

Before the application of ETR, the following activities were carried out: a) a grid was drawn over the wall as a reference for the measurements, and b) a test line to measure the contact resistance (CR) which is the initial resistance between the electrode and the wall surface. It was necessary to remove the paint layer, polish, and wet the contact surface of the electrodes until CR (Contact Resistance) was less than 10 kOhm-m. According to Leucci (31), values below 20 kOhm-m do not significantly affect the results. Subsequently, measurements were started on the drawn lines.

For the application of the ERT measurements, a Syscal Junior R1 Plus resistivity meter with 24 electrodes using dipole-dipole arrays was used. The steel bar electrodes used with this equipment for the injection of electric current were replaced by square pads for electrostimulation, as those used in the medical field, in order to protect the integrity of the walls and to apply measurements above the wall in vertical planes. To achieve a low contact resistance between the electrodes and the surface, conductive gel adhesive and clay were used on some occasions. While the gel application resulted in stains on the wall surface, the wall was repainted after the study, as the coating held no historical significance, ensuring that no residual marks were left. For the measurements in the floor, steel nails as those used in carpentry work were used as electrodes.

The ERT measurements were located on the area with the highest presence of moisture (on the right side of the wall), obtaining horizontal and vertical profiles in the wall, from left to right and from bottom to the top, respectively (Figure 5b). Six horizontal lines of 2.99 m long with electrodes every 0.13 m were carried out at different heights of the wall, while three verticals of 3.45 m long with electrodes every 0.15 m, completing the ERT arrangement with two floor lines of 4.6 m long with electrodes every 0.20 m (Figure 5a). Figure 5b illustrates the non-uniform ERT grid, with the highest density of horizontal lines concentrated in the area exhibiting visible surface moisture (marked in blue). The vertical lines were strategically placed based on the horizontal ERT data, targeting low resistivity zones that indicating wet conditions, as shown below in the results.

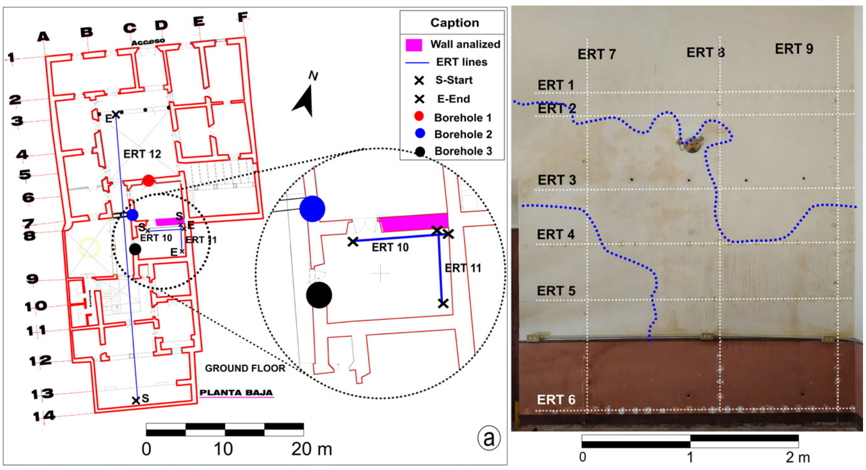

FIGURE 5. Location of ERT and boreholes lines on the plan view and on the wall. a) Floor plan with location of ERT lines and boreholes. b) ERT lines located on the wall. Lines in white correspond to electrical tomography measurements.

The floor measurements were made in the joints of the ceramic floor using nails as electrodes to generate minimum damage in the structural elements. As the research target was the subsoil under the ceramic floor cover, we used nails instead of pads to cross the ceramic cover, which is an electrically insulating material that did not allow electric current flux toward the subsoil. Two measurements were applied in order to determine the humidity conditions of the subfloor next to the wall and to identify the areas of rising humidity by capillarity (Figure 5a). In addition to the initial 9 ERT lines shown in Figure 5, Line 10 was applied parallel to the wall of interest at a 0.30 m distance, with a length of 4.6, and 0.2 m of separation between electrodes (Figure 7), while line 11 was applied with a 3.45 m length and 0.15 m spacing between electrodes, being carried out perpendicular to the wall of study, and separated at 0.42 m from the wall with D axis, see Figure 8.

Complementary to the ERT measurements, an additional longitudinal electrical profile named ERT 12 (Figure 9), permitted to recognize the subsoil under the building. This profile was carried out in 2021 as part of a study requested by the State Government from the company GEO Geofísica Aplicada a la Geotecnia.

Reference images of the wall are added to the groups of profiles obtained from the wall (ERT 1-9) and from those applied in the soil surface (ERT 10-11), in order to easily locate them and relate superficial aspects of the wall with the profiles (Figure 7, 8 and 14). In the case of ERT 12 (Figure 9), the electrical model was superimposed on the longitudinal profile of the building to locate the studied wall and reveal the subsoil moisture conditions along the corridor of Casa Terán.

Based on the 2D sections of electrical resistivity obtained from the horizontal and vertical wall measurements (ERT 1-9), a three-dimensional model was created (Figures 12c and 13a) in order to better recognize three main features: a) resistive anomalies, b) areas with the highest moisture, and c) moisture propagation patterns.

The following flowchart shows the techniques and elements used for the analysis of moisture in the adobe wall, together with the results obtained.

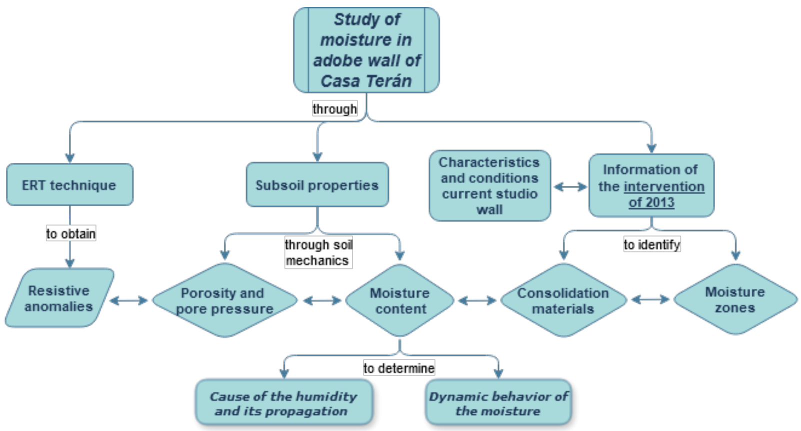

Figure 6. Flow diagram showing the techniques and elements used for the humidity analysis of the adobe wall of Casa Terán.

3. RESULTS AND DISCUSSION

3.1. Electrical Tomography in the subsoil

The moisture that can affect a building due to weather conditions depends on the level of exposure the building has to rain and solar radiation, as well as the amount of rainfall in the area where it is located. If rainwater does not infiltrate toward the building interior, the building elements most affected are typically the exterior walls and roofs, which are directly exposed to the rain.

The climate of Aguascalientes City is semi-dry, receiving an annual rainfall of 526 mm and an average annual temperature of 17.4 °C. In comparison, Mexico has an overall annual average rainfall of 777 mm, with minimum and maximum annual rainfall amounts of 250 mm and 3500 mm, respectively. This shows that Aguascalientes City is located in the region of México with the lowest quartile for rainfall, as a result, buildings in Aguascalientes City experience some of the lowest levels of exposure to rainwater in the country. Furthermore, the wall studied is inside the building, where climatic conditions remain relatively constant throughout the year, thus the contribution of climatic conditions to the moisture excess in the wall is negligible.

10 and 11 ERT profiles carried out on the floor, both present a similar configuration with values less than 500 Ohm-m. Furthermore, in both profiles, a tendency of water ascending from the subsoil towards the studied wall is observed in the area near the intersection with the D-axis (Figure 7 and 8).

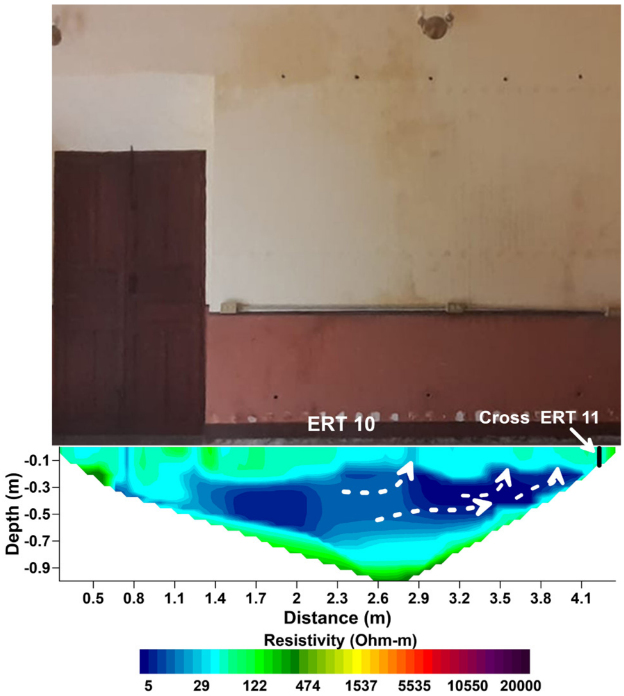

Figure 7. ERT 10 profile referenced to the wall image and parallel to the wall. This profile is located at 0.3 m from the wall of interest, see Figure 5a. In the profile of resistivity, the white dashed arrows are representing the upward water flow. The RMSE obtained in the inversion process for the profile was 11.5 %.

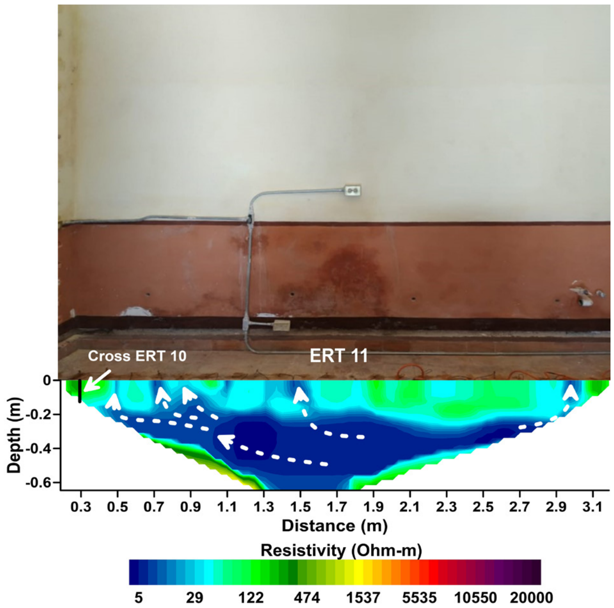

Figure 8. ERT 11 profile referenced to the wall image and perpendicular to the study wall. This profile is located at 0.42 m from the wall in axis D, see Figure 4a. In the profile of resistivity, the white dashed arrows are representing the upward water flow. The RMSE obtained in the inversion process for the profile was 8.3 %.

Profile 12 (Figure 9) is located along the corridor in the south-north direction longitudinal to the building (Figure 5a). The profile has a length of 36.8 m with a separation between electrodes of 1.6 m, limited to the dimensions of the hallway where the measurement was made. The resistivity values are in the range of 1 to 1000 Ohm-m.

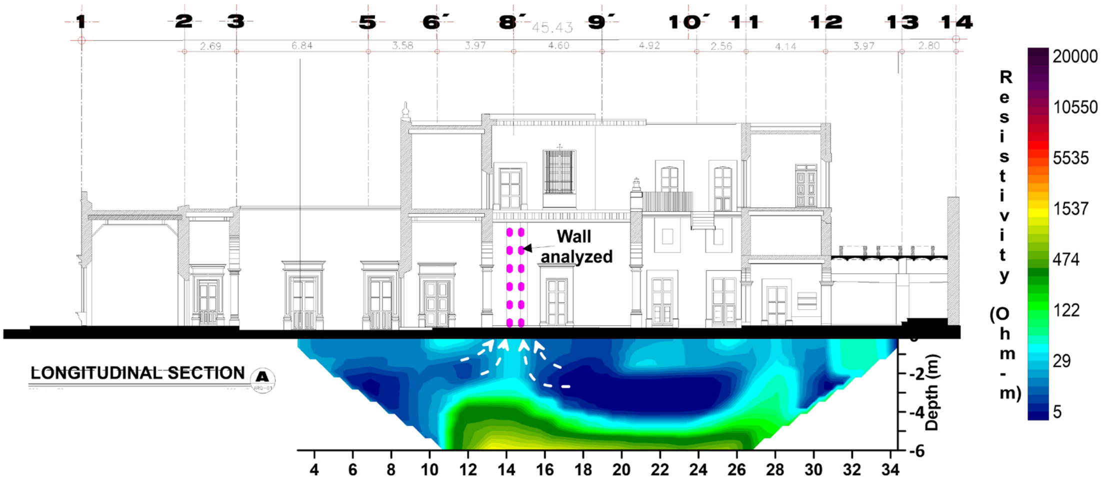

Figure 9. ERT 12 profile located along the corridor, superimposed on a longitudinal plane section of the building. The location of the study wall is indicated with a pink dashed line, while white dashed arrows in the ERT model represent the upward flow of moisture in the subsoil below the wall.

3.2. Hydraulic flow floor-wall

It is likely that the physical and hydraulic parameters obtained in the geotechnical study included in this analysis do not coincide with those present at the time of construction. Due to the historic events described early, we assume that by then the soil had a water content higher than today, with a probably saturation degree close to 100%. We also expect that the soil where the building was constructed did not receive any treatment for geotechnical improvement. Over the years, and mainly due to water extraction for urban services, the water table has dropped, and with it, the moisture content of the surface layers, which has decreased down to 58.3%, as demonstrated in the current geotechnical report.

As previously mentioned, most of the humidity issues in central Aguascalientes stem from rising damp. This phenomenon can be satisfactorily explained by the capillary action that occurs in porous materials such as adobe. However, the migration of water through the soil surface is driven by other processes, primarily involving unstable flows of water through a permeable medium. The factors contributing to this process include matric suction, osmotic suction, and the capillarity of the material. Nonetheless, practical experience indicates that the decisive factor in this phenomenon is the flow resulting from increased neutral pressure caused by an external load applied to the surface. The behavior of water flow in porous media was initially studied by Henry Darcy, who formulated Darcy's law (37). However, it was Terzaghi (38) who provided a comprehensive explanation of the physical behavior of soil and the water contained within its pores when subjected to external loads.

The behavior of loads and unsteady flow in a porous medium is explained under the following conditions: consider a soil stratum of infinite horizontal extent and thickness H, where both the solids and water are incompressible, this assumption is valid given the range of pressures exerted by structures on the soils (39). Additionally, the voids in the material are filled with free fluid, implying that the soil is fully or nearly fully saturated, and that the water can drain in all directions if unconfined. When an increase in surface stresses (Δp) is applied due to the construction of a building, the stress will be entirely supported by the fluid within the soil pores at time $t = 0$ (Figure 10a), resulting in an excess hydrostatic pressure u equal to Δp throughout the entire stratum of thickness H. Subsequently, for $t > 0$, a pressure difference will develop, creating a hydraulic gradient that causes flow to migrate in all directions through the interconnected channels in the soil structure. This will lead to a gradual transfer of load to the solid soil particles (Figure 10b) and a reduction in the excess hydrostatic pressure. This process can take several years, with the rate of transfer depending on the soil's permeability and the fluid's viscosity in the pores.

During its flow throughout the soil, the water can find points at the base of the walls (recall that there is no foundation) that encourage the upward migration, for example, small breaks left after construction or cracks caused by shear stresses in adobe blocks due to differential elastic settlements. At these points, water under excessive pressure finds a point of hydrostatic equilibrium and then continues migrating upward due to the capillarity in the wall, influenced by the medium's properties (primarily pore size and distribution).

In summary, it can be stated that:

$$\text{If } t = 0 \text{ then: } \Delta p = u \qquad [1]$$
$$\text{If } t > 0 \text{ then: } \Delta p = \Delta p' + u \qquad [2]$$

where $\Delta p'$ is the intergranular stress in the soil.
and u is the pore pressure

Figure 10 illustrates the flow behavior at two different times: at $t = 0$ (a) and $t > 0$ (b) in accordance with effective stress Terzaghi's equation. Initially, hydrostatic pressure in excess decreases as water migrates from the pores to areas with lower pore pressure, forming distinctive flow lines. The electrical tomography profiles show how moisture in the material is concentrated in areas where water can easily migrate to regions with lower stress.

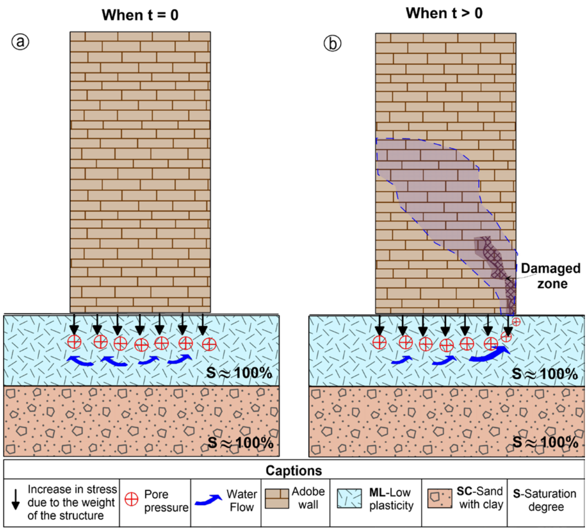

Figure 10. Variation of pore pressure and hydraulic flow due to the increase in stress when t = 0 (a) and when t > 0 (b).

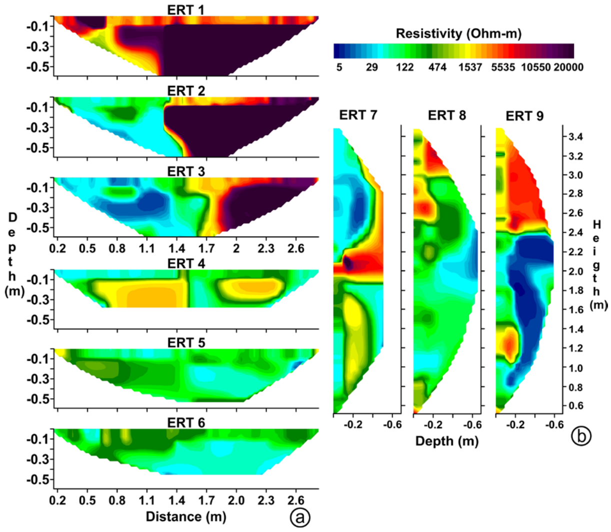

Figure 11. ERT models of horizontal and vertical measurements. a) ERT profiles 1 through 6 at 3.8, 3.5, 2.7, 1.6, 1.2, and 0. 325 m high respectively. a) Image of the dividing wall with horizontal and vertical ERT lines. b) ERT profiles 7, 8 and 9. For these profiles, electrode 1 was located in the lower part, close to the floor and electrode 24, in the upper part, close to the ceiling. The RMSE obtained in the nine profiles in the investment process was in the range of 10.9 to 8.2%.

3.3. Electrical Tomography in walls

This study presents the results obtained through the ERT techniques applied to the wall of interest. An interpretation based on the images obtained from the exposed wall is performed to identify areas with higher moisture content, determine the type of moisture present in the wall, and define anomalies associated with different materials.

The 2D profiles obtained from the wall in the horizontal and vertical directions are shown in Figure 11. The resistivity values resulted in the range of 1 to 20000 Ohm-m, while their Root Mean Squared Error (RMSE) obtained from the models was below 11%, therefore they are considered reliable resistivity models according to Leucci (31).

Figure 12 presents a photograph of the damaged wall before its repair in 2013, along with the results of the ERT measurements for interpretation. The original materials of the wall and the locations of the consolidation elements indicated as areas B in the photograph, are shown in Figure 12a. Figure 12b shows a map of the shallower electrical resistivity distribution on the wall face, produced through interpolation of the ERT profiles results, the bounds of the materials identified in the photograph of Figure 12a are pointed with dashed lines in this figure. A pseudo-3D model derived from the 2D sections shown in Figure 11 is presented in Figure 12c, which allowed identify the propagation of the moisture inside the wall.

Table 1 lists the materials identified in the photograph from Figure 12a, along with their corresponding resistivity values, which have been correlated from the 3D resistivity model shown in Figure 12c.

Table 1. Materials identified from the photographs and their corresponding resistivity values from the 3D models.

Materials	Resistivity values (Ohm-m)	Observations
Brick layers of 4x13x26 cm	100-500	Area A. Surface layer of brick in shiner course in a range of 0 to 2 m in height (Figure 3c)
Brick volumes of 7x14x28 cm	150-5000	Area B. Wall connection elements located between 0 and 2 m height.
Brick volumes of 7x14x28 cm	150-20000	Area B. Connecting elements between walls in a range 2 to 4.8 m height.
Recent adobe blocks 20x40x10 cm	150-5000	Adobe used in the reconstruction
Adobe blocks 20x60x10 cm (Clay blocks)	1-150	Original wall

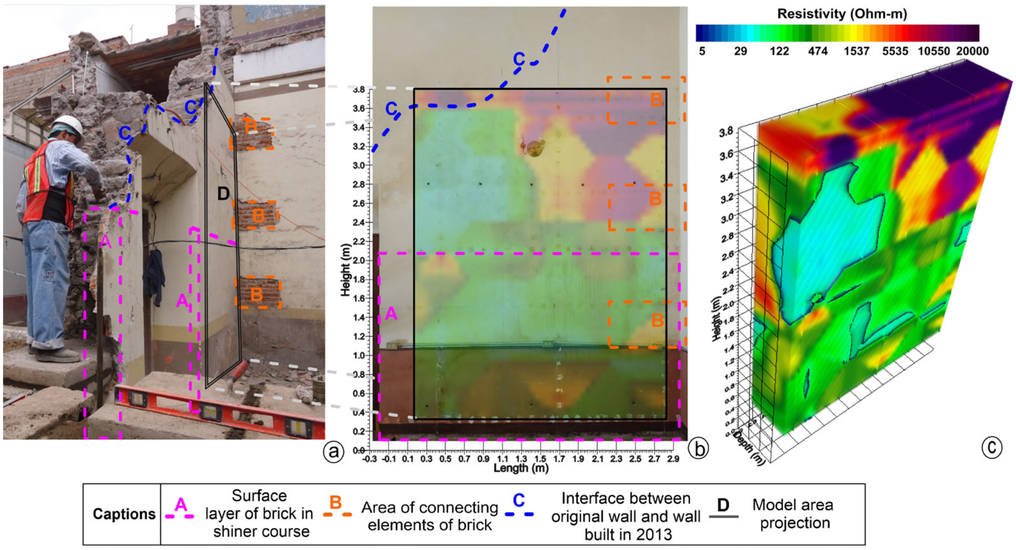

Figure 12. Integration of the information for its interpretation. a) Photograph taken during the intervention works in 2013 showing both the original wall material and the added materials. b) Studied area of the wall (rectangle D in Figure 12a) with an overlapped image of the shallower electrical resistivity produced from ERT measurements. d) Pseudo-3D electrical resistivity model of the wall elaborated from 2D ERT profiles.

In the 3D model of Figure 13, several resistive anomalies were identified, the first of them (RA1) presented resistivity values between 1 to 150 Ohm-m and identified in blue and light green colors, corresponding to the adobe of the original construction. The blue zones (1 to 20 Ohm-m) are located in the central part of the section (Figure 13 b and c) and are related to a medium with high moisture content, the cyan zones (medium moisture) surround the zones of higher moisture concentration and are located in superficial areas of the wall, highlighting zones 1 and 2 in Figure 13a. From the center of the wall toward the surface, a gradual increase in resistivity is observed, starting in the central zone of the wall with blue color and values from 1 to 20 Ohm-m and continuing in the surface with green color and values of 21 to 150 Ohm-m. A plausible explanation for this change is that the evaporation of moisture from the surface areas of the wall is causing this increase in resistivity (19, 25, 26) (Figure 13).

In Figure 14 the blue tones of the RA1 anomaly 3D models (Figure 12c and 13a) coincide with the superficial moisture stains in the ERT profiles. The 3D model shows the presence of moisture in a zone at a height near to the 3.6 m (zone 1 Figure 13a), corroborated by the stain of moisture observed in the surface of the wall moisture stain over the same zone in the image of the wall (Figure 14). Above zone 1 (Figure 13a), a drastic vertical change is observed from a low resistivity value identified in blue color (1 to 150 Ohm-m) to a high one in yellow and red colors (values above 2000 Ohm-m). This zone of change coincides with the initial level of the 2013 reconstruction (Figure 12b). Under the reconstructed area located above 3.6 m height, a small area of low resistivity is observed (Figure 12c), indicating that moisture continues ascending through the central part of the wall. The above explanation suggests that from the initial level of the reconstructed area the material has zero or low moisture content, which generates a drastic change in resistivity values. Therefore, it is inferred that before the explosion, the upper level of the moisture front in the wall was located above the 3.6 m height. The cappuccino wall layer is probably causing a reduction in the evaporation rate in the first 2 m of height, which instead is causing the moisture front to reach higher inside the wall. According to several authors (19, 29, 40) one of the factors that affect the maximum height reached by the moisture front is evaporation, in addition to the abundant flow and the relatively high permeability of the construction materials.

Evaporation is the process by which water transitions from a liquid state to a gaseous state due to increasing temperature. This process diminishes the quantity of water present in the pores of wall materials that are exposed to hot, dry air, transferring the moisture into the surrounding air as humidity.

The second anomaly (RA2) is shown in green color with values from 100 to 500 Ohm-m. This anomaly can be associated with the thin layer of bricks (shiner course) with dimensions of 0.4x0.13x0.26 m and located between the adobe and the plaster from 0 to 2 m in height (Figure 13). According to previous investigations, the resistivity of bricks saturated with salty water approaches to 20 Ohm-m, but for dry bricks the value increases up to 1,080 KOhm-m (41, 42). Therefore, the brick layer located at the bottom of the wall could present a medium of high moisture content.

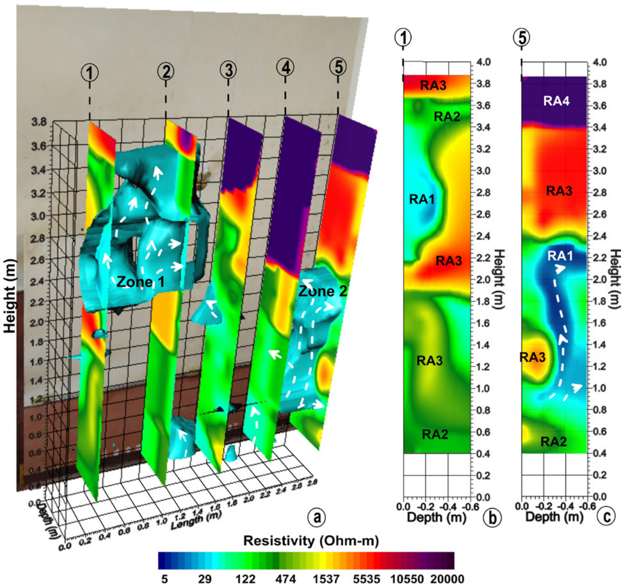

Anomalies		Section length
RA1	Blue and light green color, values of 1 to 150 Ohm-m	1. At 0.4 m
		2. At 1 m
RA2	Dark Green color, values in the range 50 a 150 Ohm-m	3. At 1.6 m
RA3	Green and yellow color, values in the range 150 a 5000 Ohm-m	4. At 2.2 m
RA4	Dark red and purple color, values greater than 5000 Ohm-m	5. At 2.8 m

Figure 13. Vertical sections located at different distances in the 3D model with the image of the wall as a reference. An envelope volume of resistivity values less than 50 Ohm-m is generated. a) Isometric 3D model with vertical sections 1-5 along the wall b) and c) Sections of greater interest. In these sections, areas with higher moisture concentration are defined. Section 1 displays the maximum height of the wet front, and Section 5 displays the initial rise of moisture in the wall. Four identified resistive anomalies (RA1-RA4) are indicated in the figure.

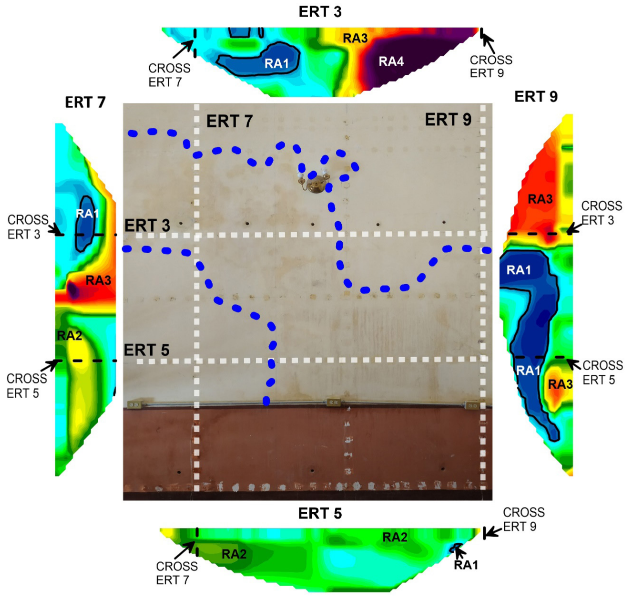

Figure 14. Image of the wall with moisture stain delimited with the two dashed blue lines as well as the horizontal and vertical ERT profiles marked with the white dashed lines. The predominant resistive anomalies (RA1 through RA4) are indicated in the ERT models.

The resistive anomaly 3 (RA3) is shown in green and yellow colors with values from 150 to 5000 Ohm-m (Figure 13). This anomaly coincides with the area of the wall-to-wall connection shown in Figure 12a. Therefore, this anomaly can be related to brick volumes with medium-to-high moisture content in the periphery of volume and its core with low moisture content located in the lower part of the wall (between 0 and 2.4 m height). Therefore, the consolidation elements located in different sections of the wall below 2.4 m are included in this anomaly (RA3). Likewise, at the height of the area reconstructed in 2013, resistivity values in the RA3 range are shown in yellow and red colors (Figure 12).

Finally, resistive anomaly 4 (RA4) is shown in purple color and located at zones higher than 2.4 m. This anomaly is associated with brick volumes with low moisture content with values larger than 5000 Ohm-m (Figure 13).

The distribution of low resistivity anomalies suggests that moisture in the wall comes from the subsoil immediately near to the wall, rising mainly on the right side of the wall, from 2.4 m in length in the 3D model, as shown in Figure 13. In the ERT models obtained from the subsoil (ERT 10, 11, and 12), a layer with high moisture content is defined below the building and is concentrated mainly in the area of patios 1 and 2, which are close to the wall under study (see Figure 9). In the case of the profiles located on the floor next to the wall of interest (ERT 10 and 11), an ascending moisture plume is observed in both profiles on the right side of the wall, indicated in Figures 7 and 8. Therefore, the most critical case of rising water is observed at the junction between the walls of axis D and the axis of the study wall (Axis 8, Figure 5). This area could present characteristics of porosity and low evaporation that favor an upward moisture flow, coinciding with the factors mentioned by Franzoni (26). According to the author, in walls having material with capillary pores and abundant moisture flow that does not evaporate, rising dampness can reach elevated heights.

The moisture problem in the wall is due to rising dampness by capillarity. As stated in the introduction, the building was constructed without foundation in the walls, thus there is no barrier to interrupt the flow of moisture into the wall. Furthermore, based on the photographic records of the interventions conducted on the wall and resistivity data, it can be deduced that the newly integrated materials in the wall exhibit low or no moisture content. This suggests that moisture gradually penetrates the inserted material over time.

Concerning the Knapen siphons placed at 0.42 m and 1.7 m height, when reviewing the 3D model (Figure 12 and 13) there is no variation in the resistivity values in the area of the tubes that indicate a change in humidity, therefore, it can be deduced that the effectiveness of these knapen siphons is low since no zones of influence (zones with humidity reduction) are defined.

4. CONCLUSIONS

Using 2D electrical tomography, we successfully identified areas with higher moisture concentration and delineated changes in the different materials comprising the wall. The 3D model, combined with electrical profiles taken from the ground and subsoil information from the soil mechanics report, indicates that the moisture present in the studied wall is primarily caused by water flow migration through the interconnected pores of the soil. This phenomenon is driven by increased pressure and capillary action, resulting in water emerging from the subsoil under the wall.

The ERT data and material identification from images obtained during the reconstruction stage in 2013 suggest that the wall has undergone several interventions over nearly 250 years. Most of these works located in the lower part and at medium height of the wall, where materials such as annealed red brick bonded with cement-sand mortar, matacán, and new adobe have been added to restore stability. These interventions have transformed the wall from having limited heterogeneity to being highly heterogeneous. This change creates flow lines between the materials in transition through which water rises variably within the wall, with a diagonal trend, as shown in the 3D model.

It is noteworthy that there is currently no research employing Electrical Resistivity Tomography (ERT) technique to study moisture in adobe walls. Additionally, to obtain more precise interpretations, it is necessary to characterize various materials under different humidity conditions, and to perform ERT surveys at different moments: in dry and in humid periods (before and after rains), subjects not yet addressed in the literature. Therefore, despite the lack of resistivity ranges associated with specific materials, the highly heterogeneous Casa Terán wall presents an interesting and valuable practical case for study.

Acknowledgements

We thank Architect José Luis García Rubalcava for his generosity in allowing us to disseminate this work. We also express our sincere thanks to the staff of the INAH Center Aguascalientes, the Cultural Institute of Aguascalientes, and the Public Works Department for their invaluable support of our research and for facilitating access to the property. Finally, we extend our gratitude to Engineer Juan Fuentes and his company GEO Geofísica Aplicada a la Geotecnia for providing us with previously conducted measurement data, which were important for the development of this work.

Authorship contribution statement

Raudel Padilla-Ceniceros: Conceptualization; Formal analysis; Investigation; Methodology; Software; Writing - original draft; Writing - review & editing.
Jesús Pacheco-Martínez: Supervision; Validation; Visualization, Writing - original draft; Writing - review & editing.
William Herbe Herrera León: Formal analysis; Methodology.
Martín Hernández-Marín: Validation; Visualization, Writing - original draft.
Rubén Alfonso López-Doncel: Validation; Visualization; Writing - original draft.
Jorge Villanueva Clavel: Investigation.
Hugo Luna-Villavicencio: Software; Writing - original draft.

Declaration of competing interest

The authors of this article declare that they have no financial, professional or personal conflicts of in-terest that could have inappropriately influenced this work.

REFERENCES

1. Mediateca - Instituto Nacional de Antropología e Historia. «Casa Terán». Accedido 30 de noviembre de 2022. Retrieved from https://mediateca.inah.gob.mx/repositorio/islandora/object/guia%3A29.

2. Bañuelos C, Maldonado S. 27 de julio de 2012. Explosión en centro cultural de Aguascalientes. La jornada. Retrieved from https://www.jornada.com.mx/2012/07/27/estados/035n1est.
3. Amoroso GG, Fasina V. 1983. Stone decay and conservation; Atmospheric pollution, cleaning; and consolidation.
4. Sandrolini F, Franzoni E. 2006. An operative protocol for reliable measurements of moisture in porous materials of ancient buildings. Build. Environ. 41(10):1372-1380. https://doi.org/10.1016/j.buildenv.2005.05.023.
5. Sass O, Viles H. 2022. Heritage hydrology: a conceptual framework for understanding water fluxes and storage in built and rock-hewn heritage. Herit Sci. 10:66. https://doi.org/10.1186/s40494-022-00693-7.
6. Mulvin L, Lewis JO. 1994. Architectural detailing, weathering and stone decay. Build. Environ. 29(1):113–138. https://doi.org/10.1016/0360-1323(94)90060-4.
7. Camuffo D. 1995. Physical weathering of stones. Sci. Total Environ. 167(1-3):1–14. https://doi.org/10.1016/0048-9697(95)04565-I.
8. Barreira E, Almeida RMSF, Delgado JMPQ. 2016. Infrared thermography for assessing moisture related phenomena in building components. Constr. Build. Mater. 110:251–269. https://doi.org/10.1016/j.conbuildmat.2016.02.026.
9. Lisø KR, Kvande T, Hygen HO, Thue JV, Harstveit K. 2007. A frost decay exposure index for porous, mineral building materials. Build. Environ. 42(10):3547-3555. https://doi.org/10.1016/j.buildenv.2006.10.022.
10. Blavier CLS, Huerto-Cardenas HE, Aste N, Del Pero C, Leonforte F, Della Torre S. 2023. Adaptive measures for preserving heritage buildings in the face of climate change: A review. Build. Environ. 245:110832. https://doi.org/10.1016/j.buildenv.2023.110832.
11. Charola AE. 2000. Salts in the deterioration of porous materials: an overview. J. Am. Inst. Conserv. 39(3):327-343. https://doi.org/10.1179/019713600806113176.
12. Siegesmund S, Weiss T, Vollbrecht A. 2002. Natural stone, weathering phenomena, conservation strategies and case studies: introduction. Geol. Soc. Spec. Publ. 205(1):1-7. https://doi.org/10.1144/GSL.SP.2002.205.01.01.
13. Siegesmund S, Snethlage R. 2014. Stone in architecture: properties, durability. Springer, Berlin, Heidelberg. https://doi.org/10.1007/978-3-642-45155-3.
14. Gentilini C, Franzoni E, Bandini S, Nobile L. 2012. Effect of salt crystallisation on the shear behaviour of masonry walls: an experimental study. Constr. Build. Mater. 37:181-189. https://doi.org/10.1016/j.conbuildmat.2012.07.086.
15. Siedel H. 2018. Salt efflorescence as indicator for sources of damaging salts on historic buildings and monuments: a statistical approach. Environ. Earth Sci. 77:572. https://doi.org/10.1007/s12665-018-7752-4.
16. Franzoni E, Sassoni E. 2011. Correlation between microstructural characteristics and weight loss of natural stones exposed to simulated acid rain. Sci. Total Environ. 412-413:278-285. https://doi.org/10.1016/j.scitotenv.2011.09.080.
17. Johnson JB, Haneef SJ, Hepburn BJ, Hutchinson AJ, Thompson GE, Wood GC. 1990. Laboratory exposure systems to simulate atmospheric degradation of building stone under dry and wet deposition conditions. Atmos. Environ. Part A. 24(10):2585-2592. https://doi.org/10.1016/0960-1686(90)90136-B.
18. Warscheid T, Braams J. 2000. Biodeterioration of stone: a review. Int. Biodeterior. Biodegrad. 46(4)343–368. https://doi.org/10.1016/S0964-8305(00)00109-8.
19. Franzoni E. 2014. Rising damp removal from historical masonries: A still open challenge. Constr. Build. Mater. 54:123–136. https://doi.org/10.1016/j.conbuildmat.2013.12.054.
20. Jiménez-González I, Rodríguez-Navarro C, Scherer GW. 2008. Role of clay minerals in the physicomechanical deterioration of sandstone. J. Geophys. Res. Earth Surf. 113(F2). https://doi.org/10.1029/2007JF000845.
21. Sandrolini F, Franzoni E, Cuppini G. 2000. Predictive diagnostics for decayed ashlars substitution in architectural restoration in Malta. Mater. Eng. Modena. 11(3):323-338.
22. Gómez Serrano J. 2015. Remansos de ensueño. Las huertas y la gestión del agua en Aguascalientes, 1855-1914. Hist. Mex. 64(3):1001–1097. Retrieved from https://www.scielo.org.mx/scielo.php?script=sci_arttext&pid=S2448-65312015000101001
23. Indekeu ML, Feng C, Janssen H, Woloszyn M. 2021. Experimental study on the capillary absorption characteristics of rammed earth. Constr. Build. Mater. 283:122689. https://doi.org/10.1016/j.conbuildmat.2021.122689.
24. Zhang X, Nowamooz H. 2021. Effect of rising damp in unstabilized rammed earth (URE) walls. Constr. Build. Mater. 307:124989. https://doi.org/10.1016/j.conbuildmat.2021.124989.
25. Amoroso GG, Camaiti M. 2002. Trattato di scienza della conservazione dei monumenti: etica della conservazione, degrado dei monumenti, interventi conservativi, consolidanti e protettivi (Vol. 54). Alinea Editrice.
26. Franzoni E. 2018. State-of-the-art on methods for reducing rising damp in masonry. J. Cult. Herit. 31:S3–S9. https://doi.org/10.1016/j.culher.2018.04.001.
27. Giaccone D, Santamaria U, Corradi M. 2020. An experimental study on the effect of water on historic brickwork masonry. Heritage. 3(1):29–46. https://doi.org/10.3390/heritage3010003.
28. Franzoni E, Berk B, Bassi M, Marrone C. 2023. An integrated approach to the monitoring of rising damp in historic brick masonry. Constr. Build. Mater. 370:130631. https://doi.org/10.1016/j.conbuildmat.2023.130631.
29. Rirsch E, Zhang Z. 2010. Rising damp in masonry walls and the importance of mortar properties. Constr. Build. Mater. 24(10):1815–1820. https://doi.org/10.1016/j.conbuildmat.2010.04.024.
30. Loke MH. 1999. Electrical imaging surveys for environmental and engineering studies. A practical guide to. 2:70.
31. Leucci G. 2019. Nondestructive Testing for Archaeology and Cultural Heritage: A Practical Guide and New Perspectives. Springer International Publishing, Cham. https://doi.org/10.1007/978-3-030-01899-3.

32. INAH file. ca. 2013. Fotos Casa Terán por semana 2013 [fotografías inéditas]. Archivo INAH.
33. ASTM International. 2017. ASTM D4318-17e1 Standard test methods for liquid limit, plastic limit, and plasticity index of soils. https://doi.org/10.1520/D4318-17
34. ASTM International. 2017. ASTM D6913/D6913M-17 Standard test methods for particle-size distribution (gradation) of soils using sieve analysis. https://doi.org/10.1520/D6913_D6913M-17
35. ASTM International. 2017. ASTM D4959 Standard test method for determination of water (moisture) content of soil by direct heating. Retrieved from https://www.astm.org/d4959-00.html
36. ASTM International. 2017. ASTM D2487-17 Standard practice for classification of soils for engineering purposes (unified soil classification system). Retrieved from https://www.astm.org/d2487-17.html
37. Darcy H. 1856. Les Fontaines publiques de la ville de Dijon (Public fountains of the city of Dijon). Paris: Dalmont.
38. Terzaghi K. 1925. Erdbaumechanik auf bodenphysikalischen grundlagen. Deuticke, Wien.
39. Juárez Badillo E, Rico Rodríguez A. 2001. Mecánica de suelos (Tomo I). Limusa, México DF.
40. Clifton JR, Davis F. 1979. Protecting adobe walls from ground water. National Bureau of Standards, Gaithersburg, MD.
41. Abu-Zeid N, Botteon D, Cocco G, Santarato G. 2006. Non-invasive characterisation of ancient foundations in Venice using the electrical resistivity imaging technique. NDT & E Int. 39(1):67–75. https://doi.org/10.1016/j.ndteint.2005.06.007.
42. Kuranchie FA, Shukla SK, Habibi D. 2014. Utilisation of iron ore mine tailings for the production of geopolymer bricks. Int. J. Min. Reclam. Environ. 30(2):92–114. https://doi.org/10.1080/17480930.2014.993834.